Journal of the Korean Physical Society, Vol. 50, No. 5, May 2007, pp. 1332∼1339

Investigation of Solid-State Photomultipliers for Positron Emission Tomography Scanners

Jae Sung Lee
Department of Nuclear Medicine, College of Medicine, Seoul National University, Seoul 110-744

Mikiko Ito, Kwang-Souk Sim, Byungsik Hong and Kyung Sei Lee
Department of Physics, Korea University, Seoul 136-701

Jamil Muhammad and June Tak Rhee
Department of Physics, Konkuk University, Seoul 143-701

Geon Song Lee and Kwang Suk Park
Department of Biomedical Engineering, College of Medicine, Seoul National University, Seoul 110-744

In Chan Song
Department of Diagnostic Radiology, College of Medicine, Seoul National University, Seoul 110-744

Seong Jong Hong*
Neuroscience Research Institute and Division of Biological Sciences, Gachon University of Medicine and Science, Inchon 405-760

(Received 31 January 2007)

Solid-state devices to detect photons are under active research and development because they, unlike photomultiplier tubes (PMT), can be used under high-magnetic-field and radio-frequency environments, such as in magnetic resonance imaging (MRI) scanners. In addition, some of the solid-state devices have a higher particle detection efficiency and only a slightly less gain than PMTs, currently the first choice to detect photons in positron emission tomography (PET) scanners. We have tested solid-state photomultipliers (SSPM) among several different solid-state devices in the market. This paper describes the test methods and the characteristics of SSPMs with an emphasis on use in PET scanners. We obtained a 25 % energy resolution and a 4.5-ns time resolution with ^{22}Na and lutetium yttrium oxyorthosilicate (LYSO), both full-width at half maximum (FWHM). The number of fired mini-cells and the amplification factor were, respectively, estimated to be 154 $\pm$ 37 for ^{22}Na and (3.8 $\pm$ 0.9) $\times$ 10^5. Even though SSPM-LYSO couplings resulted in worse performances than PMT-LYSO couplings, the solid-state devices have good potential for use in the PET scanners, especially in combined PET/MRI scanners because the new solid-state devices appear to have better characteristics, such as a higher quantum efficiency and a larger number of mini-cells, than the tested SSPMs.

PACS numbers: 87.58.Fg
Keywords: Solid-state photomultiplier, PET, LYSO, Energy resolution, Time resolution, MRI

I. INTRODUCTION

Positron emission tomography (PET) scanners which enable quantitative measurements of physiological indications by in-vivo imaging of biochemical substances in the body have been used for investigations of biochemical and pathological phenomena, diagnosis of disease, and judgement of prognosis after treatment. Imaging apparati providing anatomical information, for example, computed tomography (CT) and magnetic resonance imaging (MRI) scanners, are being added to PET scanners with an excellent functional imaging [1]. A combined PET/CT system in which PET provides functional in-

*E-mail: hongseongj@gachon.ac.kr; Fax: +82-32-460-8230

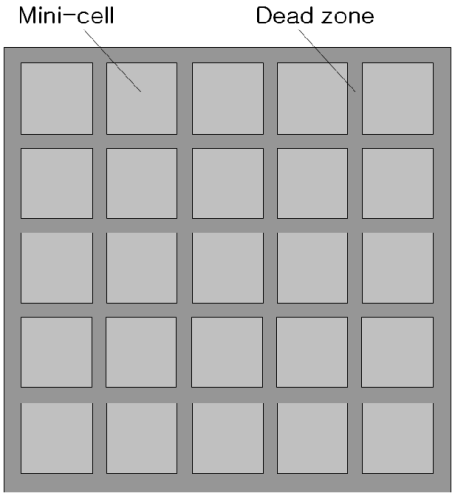

Fig. 1. Pixel matrix of the SSPM.

formation and CT gives anatomical information is being widely used. MRI has a superb capability for distinguishing white-matter from grey-matter in the brain and for distinguishing high soft-tissue contrast, for which CT has a limited capability. In addition, MRI is not harmful to subjects, unlike CT which has to use a high dose of X-rays to achieve a high resolution. A major obstacle of a combined PET/MRI system with photomultiplier tubes (PMT) is that PMTs are extremely sensitive, even to very low magnetic fields of a few tens of gauss. Even though avalanche photodiodes (APD) have been successfully incorporated into the combined PET/MRI system [2,3], current APDs have low gains of several hundreds, requiring elaborate preamplifiers.

High-energy-physics experiments need to measure the energies of various particles, such as photons, electrons, and jets with scintillating materials to study various physics phenomena, such as searches for new particles and physics beyond the standard model. Since these experiments typically require a large number of channels, the devices have to be relatively inexpensive. A future e^+ e^- collider may require finely segmented scintillating detectors under a high magnetic field to resolve the jets [4]. Because of these requirements, high-energy-physics communities have been developing solid-state devices to replace PMTs [5].

Several solid-state devices to detect photons are being developed by several companies under various product names, such as Geiger-mode photodetectors (GMPD), solid-state photomultipliers (SSPM), silicon photomultipliers (SiPM), and multi-pixel photon counters (MPPC). All these devices consist of many mini-cells, as shown in 1, ranging a few hundred to a few thousand mini-cells, each of which, when struck by a photon, generates an avalanche of electrons.

Some of these devices have promising characteristics of a relatively high gain ($\sim 10^6$), a high particle detection efficiency (20 $\sim$ 50 %) at an $\sim$420 nm photon wavelength.

Table 1. Specifications of the SSPM (SSPM-0604BE-CER).

Parameter	Units	Typical Values
Peak sensitivity wavelength	nm	690
Single photon detection efficiency	%	10 at 400 nm
Operating voltage	V	53 – 58
Typical gain		0.5×10^6
Signal time	ns	5
Number of mini-cells		556

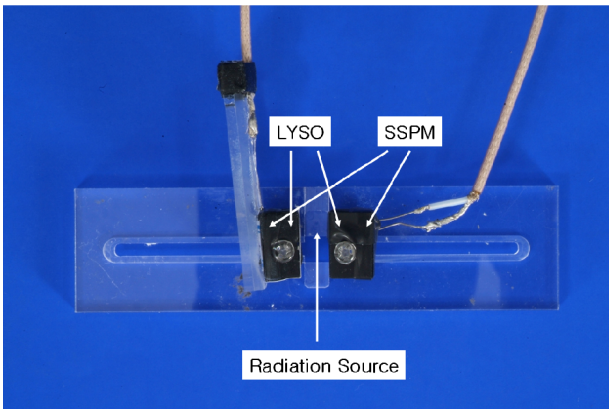

Fig. 2. Lucite structure to fix the SSPM-LYSO couplings and the radiation source. Each SSPM-LYSO coupling was inserted into a small piece of lucite structure wrapped with black tape to shield it from external light.

Recently, the SiPM has been demonstrated a feasibility for use as readout elements in scintillator-based PET scanners, obtaining an energy resolution of about 22 % and a coincidence time resolution of 2.1-ns [6]. The solid-state devices that we have tested were SSPMs obtained from Photonique SA in Switzerland [7]. The specifications given by the vendor are shown in Table 1.

The structure of this paper is as follows: We first describe a test setup, and then the energy and coincidence time resolutions of PMT-LYSO couplings exposed to a ^{22}Na positron source. Next the characteristics of SSPM pulses are compared with those of PMT pulses. After estimating the quantity of charges generated by a single mini-cell exposed to one or more photons, we obtain the SSPM gain at the operating voltage. We then present the energy and coincidence time resolutions of SSPM-LYSO couplings exposed to various radiation sources, such as ^{133}Ba, ^{22}Na, ^{137}Cs, and ^{18}F. After describing the rate dependency of the energy and coincidence time resolutions, we summerize our main results in the conclusion.

II. TEST SETUP

We made a Lucite structure for a fixture of SSPMs coupled to LYSO crystals and a radioactive source as

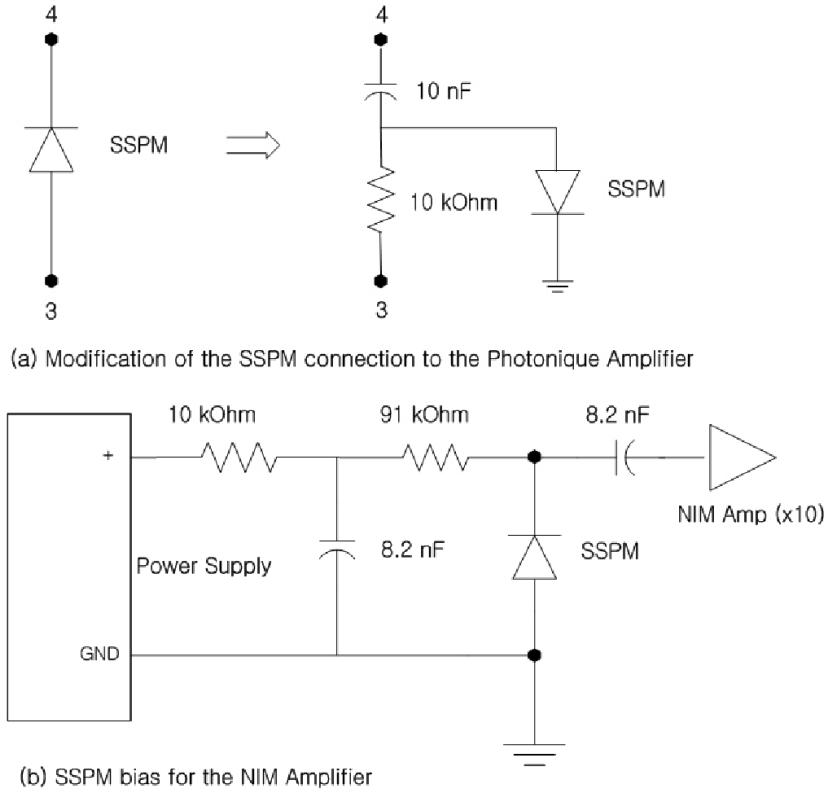

Fig. 3. Circuit diagram to test the SSPMs.

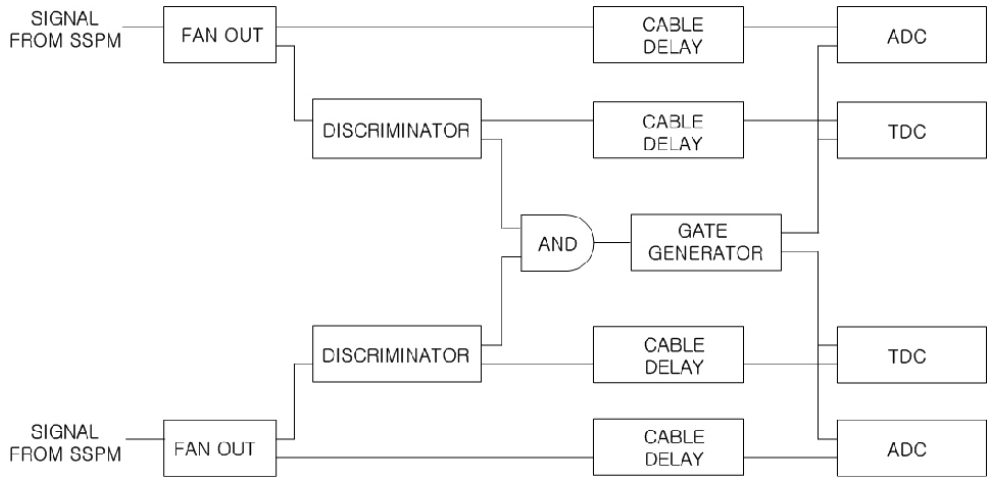

Fig. 4. Schematic diagram of the data flow.

shown in Figure 2. The LYSO crystals with dimensions of 1.5 mm × 1.5 mm × 7.0 mm were wrapped with three layers of 3M enhanced spectral reflector (ESR) polymer except for the surface facing the SSPMs. Optical grease (BC-630) with a refractive index of 1.463 from Saint Gobain was applied to the interface between the SSPM and the crystal. A radioactive source was placed between the two SSPM-LYSO couplings.

The circuit diagram shown in Figure 3 was used to apply the bias voltage to the SSPMs. Since the amplifier obtained from Photoniuqe SA in Switzerland resulted in positive signals, we added an extra capacitor and resistor as shown in Figure 3(a) to invert the signal so that the signal could be used with a VME/NIM system. Figure 3(b) shows the circuit diagram to bias the SSPMs to be used with the CAEN NIM amplifier. Figure 4 shows the data flow diagram of the test setup. Two different kinds of discriminators were used to produce NIM signals, which were later used to generate ADC GATE, TDC START, and STOP pulses. Unless stated other-

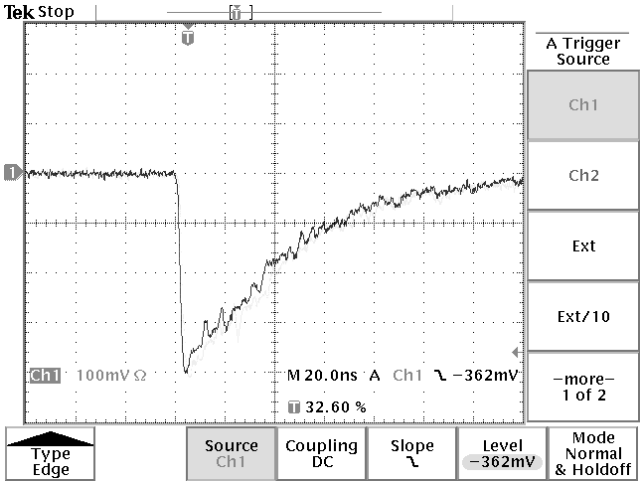

Fig. 5. Raw pulse from the Hamamatsu H2431-50 PMT mounted with a single LYSO crystal.

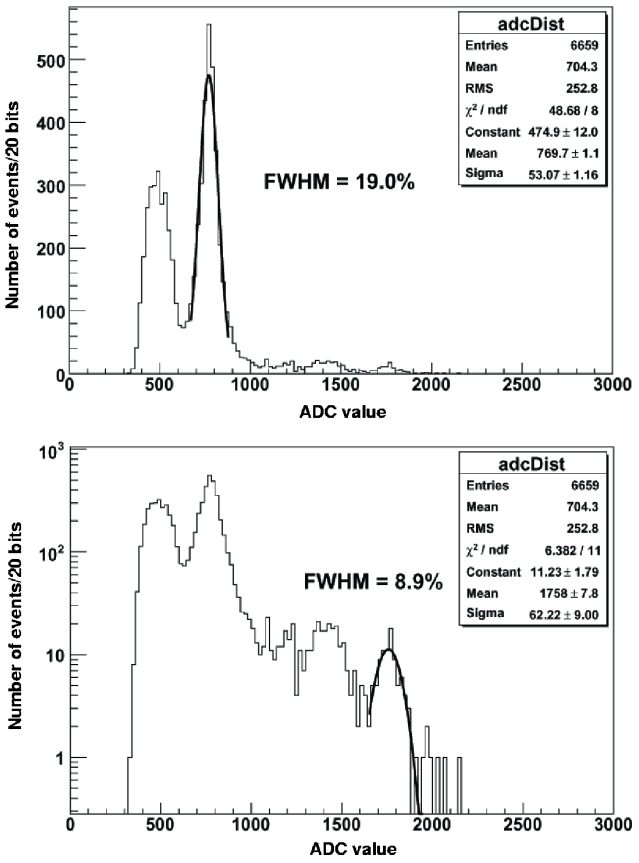

Fig. 6. ADC distributions obtained from the Hamamatsu H2431-50 PMT coupled to a single LYSO crystal. One ADC bit corresponds to 200 fC. A pedestal value of 112 has been taken into account to obtain the energy resolution. The pedestal value was obtained by measuring the ADC values with random triggers.

wise, a 300-ns GATE width was used to obtain ADC values. Appropriate lengths of cables were added to ensure that signals arrived within the ADC GATE and that the TDC START pulses arrived before the TDC STOP pulses. We used a CAEN V965 VME ADC module, which measures integrated charge up to 800 pC with a 200 fC/bit resolution. To measure the arrival time differences between START and STOP pulses, we used a CAEN V775N VME TDC module, which measures time differences up to 140 ns with a 35 ps/bit resolution. To compare coincidence time resolutions, we tried two different kinds of discriminators, namely a CAEN N415A constant fraction discriminator and a CAEN N840 level discriminator. The same data flow shown in Figure 4 was also used to measure the energy and time resolutions of the PMT-LYSO couplings.

III. RESULTS

1. Energy and Time Resolutions of PMT-LYSO Couplings

We measured the energy and time resolutions of the PMT-LYSO couplings to verify the test setup and compared these resolutions with the resolutions of the SSPM-LYSO couplings. Each LYSO crystal was wrapped with three layers of 3M ESR polymer except for the surface facing the Hamamatsu PMT [8]. Each LYSO crystal was mounted to a Hamamatsu PMT with optical grease (BC-630) of refractive index 1.463. One Hamamatsu H2451-50 PMT was mounted with a single 1.5 mm × 1.5 mm × 7.0 mm LYSO crystal, and the other Hamamatsu E5859-03 PMT was mounted with a 4 × 4 array of 2.0 mm × 2.0 mm × 7.0 mm LYSO crystals. Figure 5 shows a typical pulse from the PMT mounted with the single crystal. The pulse was captured with a Tektronix TDS 3052B oscilloscope, requiring coincidence of two PMT signals, with the 3.0×10^5 Bq ^{22}Na source between the PMT-LYSO couplings. The voltages applied to the Hamamatsu H2451-50 and the E5859-03 PMTs were, respectively, −1800 V and +1100 V.

Coincidence signals from the two PMT-LYSO couplings were used to obtain the ADC and the TDC values of the signals with a 250-ns GATE width and −35-mV discriminator levels. Figure 6 shows an ADC distribution from the H2451-50 PMT mounted with a single crystal with an energy resolution of 19 %, as obtained with a Gaussian fitting near the 511-keV photoelectric peak. The lower figure of Figure 6, with a log y-scale, also shows the photoelectric peak of 1.295-MeV photons emitted from ^{22}Na, with an energy resolution of 8.9 %. Figure 7 shows a TDC distribution with a coincidence time resolution of 0.73 ns obtained with the constant fraction discriminator. Events in the TDC distribution in Figure 7 were required to have ADC values around the 511-keV photoelectric peaks for both PMT-LYSO couplings. A similar test with the level discriminator resulted in a

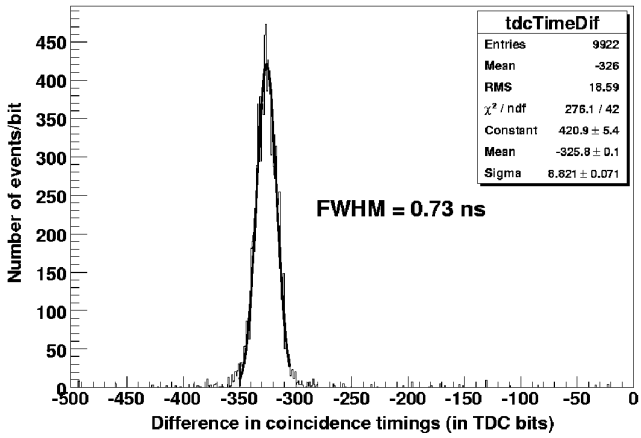

Fig. 7. TDC distribution of the PMT-LYSO coupling using the CAEN NIM constant fraction discriminator. One TDC bit corresponds to 35 ps.

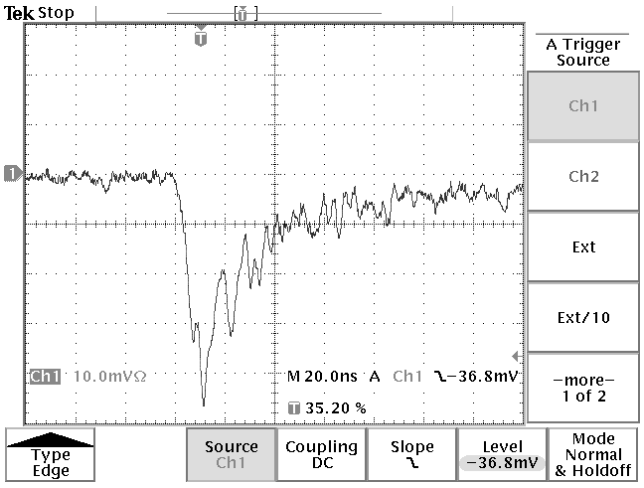

Fig. 8. Raw pulse from the SSPM mounted with a single crystal.

0.96-ns time resolution. The excellent time resolution is due to the fast rise time of the PMT, as shown in Figure 5. The Hamamatsu H2431-50 and E5859-03 PMTs have rise times of 0.7 ns and 2.6 ns, respectively.

2. Characteristics of SSPM Raw Signals

Because of the mini-cell structure of the SSPM shown in Figure 1, a raw pulse from a SSPM is given by the sum of individual pulses from individual mini-cells exposed to photons. Figure 8 shows a raw pulse captured with the Tektronix oscilloscope and required a coincidence of two SSPM-LYSO couplings exposed to the ^{22}Na radioactive source. The raw pulse shown in Figure 8 consists of overlapping multiple short pulses, as expected, and shows a slower rise time than the PMT raw pulse in Figure 5.

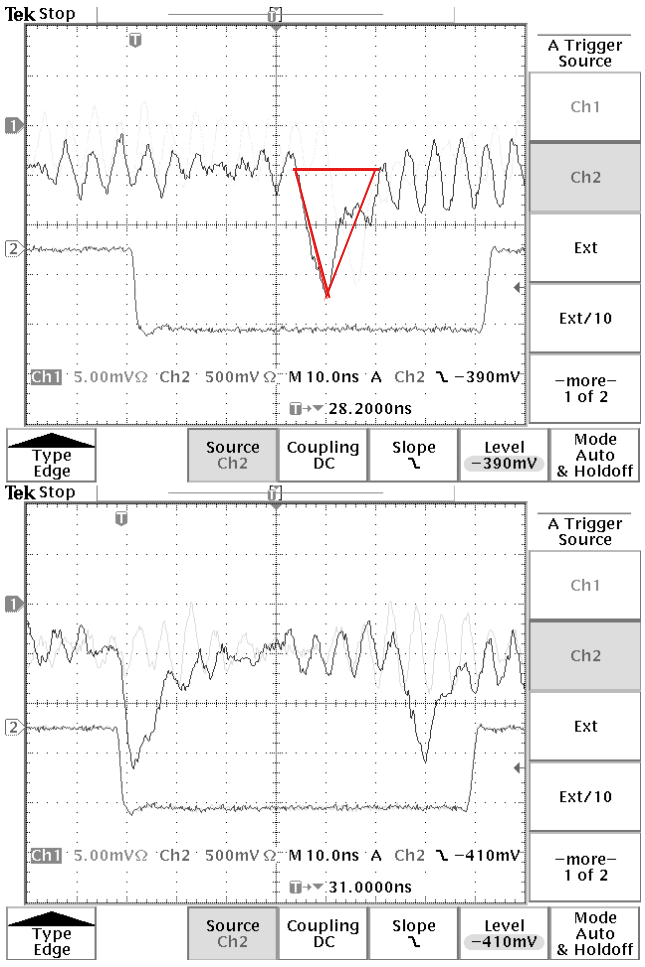

Fig. 9. Single mini-cell pulses captured with the Tektronix oscilloscope. The area inside the triangle was used to calculate the quantity of the charges.

3. Charges Generated by a Single Mini-cell Signal

Figure 9 shows single mini-cell signals captured with the Tektronix oscilloscope by triggering a signal generated with a Tektronix AF320 pulse generator. These SSPM signals were obtained with a 57-V bias voltage and the Photonique amplifier biased to 5 V. The pulse generator generated a 100-Hz NIM pulse which was then used to generate a 70-ns GATE pulse as shown in Figure 9. Since no smaller signals other than noises were observed in the oscilloscope, we are confident that the signals in Figure 9 are, indeed, produced by a single mini-cell. Using the 50-Ω input impedance of the oscilloscope and Ohm's law, we estimated the quantity of charges generated by the single mini-cell to be ∼2.0 pC. We also measured the charges of single and double mini-cells by using the VME ADC. Figure 10 shows the ADC distributions, where the highest peak corresponds to the pedestal and the other peaks represent signals for firings of one and two mini-cells. Since a linear fit of these three

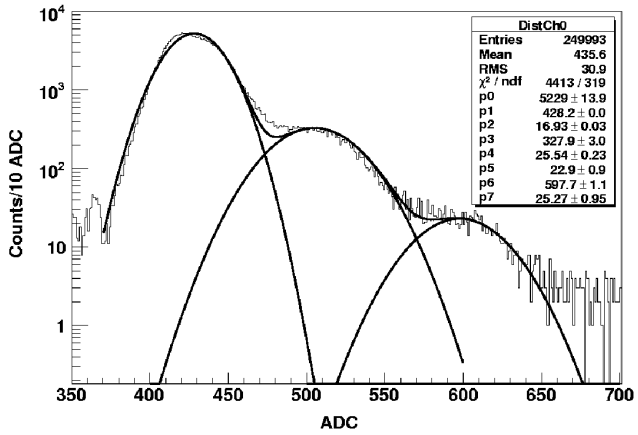

Fig. 10. ADC distributions of the pedestal, the single and the double mini-cell signals. To obtain a good fit to the data with three Gaussian distributions, we fixed the peak position of the single mini-cell signal to 505, which had been obtained in an individual Gaussian fit between 480 and 560. One bit corresponds to 25 fC.

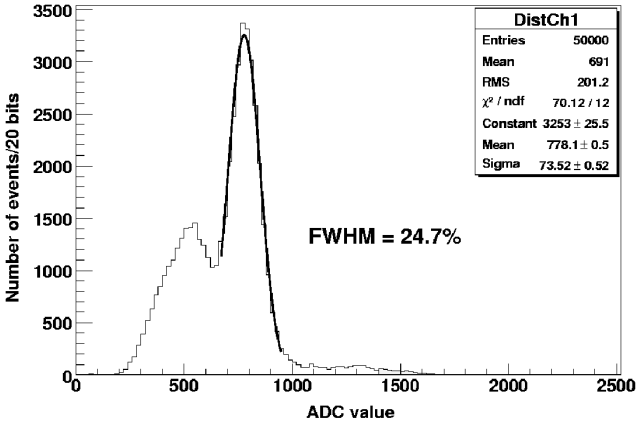

Fig. 11. ADC distribution with the CAEN NIM amplifier with a fixed gain of 10. One ADC bit corresponds to 200 fC. The pedestal value of this measurement was 77.

data points resulted in a slope of 84.5 ± 7.0, the charge generated by the single mini-cell was estimated to be 2.1 ± 0.5 pC, where the error was obtained by quadratically subtracting the pedestal width from the average width of the single and the double mini-cell ADC distributions in Figure 10.

4. Gain

One of the advantages of a SSPM is the relatively high gain of $\sim 5 \times 10^5$ at operating voltages. We estimated the gain by assuming that a single mini-cell signal was caused by one electron-hole pair and was amplified during the avalanche process in the mini-cell. The amplified signal in the SSPM min-cell was then further amplified by the Photonique amplifier to give a charge of

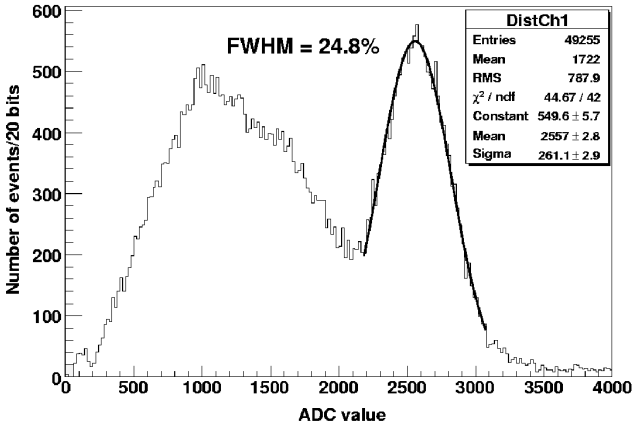

Fig. 12. ADC distribution with the Photonique amplifier with a pedestal value of 72. One ADC bit corresponds to 200 fC.

2.1 ± 0.5 pC for the single mini-cell signal. The gain of the Photonique amplifier at a 5-V bias voltage was obtained by using the photoeletric peak obtained with the CAEN NIM N979 amplifier, which has a fixed gain of 10. Figures 11 and 12, respectively, show the ADC distributions obtained with the CAEN NIM N979 and the Photonique amplifiers. The voltage applied to the SSPMs was 58 V. The gain of the Photonique amplifier was estimated to be 35, comparing pedestal-subtracted peak positions of 701 for the NIM amplifier and of 2485 for the Photonique amplifier. Using the 2.1 ± 0.5 pC charge quantity of the single mini-cell signal and the Photonique amplifier gain of 35 resulted in a SSPM gain of $(3.8 \pm 0.9) \times 10^5$. The energy resolutions of the two ADC distributions were 25 % for both amplifiers.

5. Energy Resolution

As Figure 12 shows, the energy resolution for a LYSO with a size of 1.5 mm × 1.5 mm × 7.0 mm was 25 % with the Photonique amplifier. This energy resolution is worse than the 22 % reported in Ref. 6 in which a light-mirror cone was inserted, for better collection of scintillation photons, between the SiPM and a LSO crystal with a size of 2.0 mm × 2.0 mm × 10.0 mm. We also tested energy-dependent resolutions and linearity in energy with ^{133}Ba (335 keV), ^{22}Na (511 keV), and ^{137}Cs (661 keV) radioisotopes. To prevent ADC saturation in the VME ADC module, we applied only 57 V to the SSPMs in this test. Data were taken with a self-trigger mode for all these radioisotopes, with a −35-mV threshold set to the discriminator. The energy resolution gets better as the energy of the incident γ photon increases, generating more scintillation photons in the LYSO crystals. The energy resolutions were 39.1 % for ^{133}Ba, 29.7 % for ^{22}Na, and 23.6 % for ^{137}Cs. The energy resolution for ^{22}Na became worse due to the lower voltage

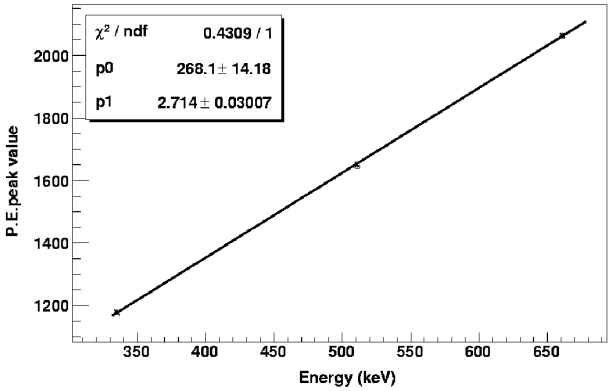

Fig. 13. Peak ADC value as a function of γ energy.

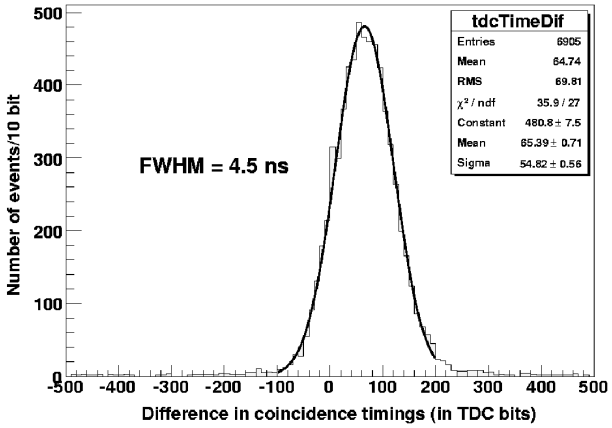

Fig. 14. Coincidence time distribution with the N415A constant fraction discriminator. One TDC bit corresponds to 35 ps.

applied to the SSPMs. Figure 13 shows the ADC values corresponding to the photopeaks obtained with these radiation sources as a function of the incident γ energy, and shows good linearity in the tested range. The better energy resolution for higher γ energies and the good linearity in energy show that the number of fired mini-cells must be smaller than the number of mini-cells in the SSPM.

6. Number of Fired Mini-cells

Since the tested SSPM has a only 556 mini-cells/mm^2, it is important to estimate the number of fired mini-cells. If the number of incident photons is small, each single photon is likely to enter into a single mini-cell. However, too many incident photons would cause more than one photon to enter the same mini-cell, losing the proportionality to the incident γ energy. Since the charge quantity of a single fired mini-cell is 2.1 $\pm$ 0.5 pC, the photoelectric peak charge quantity of 324 pC at the middle point in Figure 13 corresponds to 154 $\pm$ 37 fired mini-cells for ^{22}Na. The expected numbers of the fired mini-cells were 110 $\pm$ 26 for ^{133}Ba and 196 $\pm$ 47 for ^{137}Cs, which were obtained by scaling the γ energies emitted by the isotopes with the 511-keV for ^{22}Na. The good linearity in the tested range and the better energy resolution for ^{137}Cs than for ^{22}Na are not surprising with these numbers of fired mini-cells.

7. Time Resolution

Since the ~10-ns rise time of the SSPM signal, as shown in Figure 8, is far slower than the 1 ~ 2-ns rise time of the PMT signal, as shown in Figure 5, the SSPM time resolution may not approach the PMT time resolution of 0.73 ns shown in Figure 7. Figure 14 shows a coincidence time distribution with a resolution of 4.5 ns. A similiar test with the conventional level discriminator resulted in a coincidence time resolution of ~6.8 ns. Reference 6 reported an excellent coincidence time resolution of 2.1 ns and even mentioned the possibility of using conventional level discriminators instead of constant fraction discriminators. However, SSPM raw signals such as in Figure 8, because of their slow rise times, indicate a possibility of worse time resolution for a SSPM than the reported value of 2.1 ns for a SiPM.

8. Rate Dependency

We used a ^{18}F radioactive source to study any change in the energy and the coincidence time resolutions with the incident γ photon rate. A PET system with a 100-mm diameter is expected to result in a 2.4 $\times$ 10^4 photons/mm^2 of 511-keV γ particles when a 3.7 $\times$ 10^8 Bq ^{18}F source is positioned at the center of the PET system. Since the crystals in the test setup was separated by 6 mm, a 1.3 $\times$ 10^6 Bq ^{18}F source was required to achieve the 2.4 $\times$ 10^4 photons/mm^2. Even though the test began with an activity of 5.1 $\times$ 10^7 Bq and stopped at an activity of 1.6 $\times$ 10^6 Bq, the energy and time resolutions didn't change noticeably during the test.

IV. SUMMARY AND CONCLUSIONS

We have investigated SSPMs with an emphasis on use in PET scanners. We obtained a 25 % FWHM energy resolution and a 4.5-ns FWHM time resolution with ^{22}Na and LYSO. The number of fired mini-cells and the amplification factor were, respectively, measured to be 154 $\pm$ 37 for ^{22}Na and (3.8 $\pm$ 0.9) $\times$ 10^5. We have shown that SSPMs have a good linear energy response up to 197 $\pm$ 47 fired mini-cells out of 556 mini-

cells/mm^2 and do not show any degradation of energy and time resolutions for the incident γ flux range of a typical PET application. We find that the constant fraction discriminator gives a better time resolution than the conventional level discriminator. It would be interesting to see if new solid state devices would give an ∼2-ns coincidence time resolution comparable to the APD-LSO readout [9]. We conclude that solid-state devices have good potential for use with PET scanners, especially for combined PET/MRI scanners, because new solid-state devices with ∼1500 mini-cells/mm^2 are expected to have an ∼25 % particle detection efficiency at 420 nm [8] .

ACKNOWLEDGMENTS

We acknowledge a grant from the Basic Research Program (R01-2006-000-10296-0) of the Korean Science and Engineering Foundation (KOSEF).

REFERENCES

[1] T. F. Massoud and S. S. Gambhir, Genes & Development **17**, 545 (2003); R. Weissleder and U. Mahmood, Radiology **219**, 316 (2001).
[2] B. J. Pichler *et al.*, J. Nucl. Med. **47**, 639 (2006).
[3] M. S. Judenhofer *et al.*, in *Proceedings of IEEE NSS-MIC M08-6* (San Diego, California, 2006).
[4] D. Beznosko *et al.*, Nucl. Instrum. Meth. A **545**, 727 (2005).
[5] B. Dolgoshein *et al.*, Nucl. Instrum. Meth. A **504**, 48 (2003); D. Bisello *et al.*, *ibid.* **367**, 212 (1995); V. Golovin *et al.*, *ibid.* **518**, 560 (2004).
[6] A. N. Otte *et al.*, Nucl. Instrum. Meth. A **545**, 705 (2005). The time resolution in this paper is given for a single detector channel, requiring multiplication by $\sqrt{2}$ to obtain the coincidence time resolution.
[7] http://www.photonique.ch.
[8] http://www.hamamatsu.com.
[9] B. J. Pichler *et al.*, Phys. Med. Biol. **49**, 4305 (2004).